Journal of International Scientific Publications: Materials, Methods and Technologies

Volume 8, ISSN 1314-7269 (Online), Published at: http://www.scientific-publications.net

TRANSFORMATION OF MICROSTRUCTURE AND TEXTURE IN ALUMINUM 7475 ALLOY DURING SUPERPLASTIC FORMING

A. Blander[1], J. Szpunar[2] and Y. Takayama[3]

[1]Department of Mining and Materials Engineering, McGill University, Montreal,

Qc, H2A 2B2, Canada

[2]Department of Mechanical Engineering, University of Saskatchewan, Saskatoon, Canada

[3]Department of Mechanical Systems Engineering, Utsunomiya University, Utsunomiya, Japan

Abstract

The process of superplastic forming in 7475 aluminum alloy was analyzed using orientation imaging microscopy (OIM), X-ray diffraction (XRD) and scanning electron microscopy (SEM). These techniques were used to determine the effect of the superplastic forming on texture, grain boundary character distribution (GBCD), grain size, residual stress and microstructure at different stages of the deformation of specimens deformed in tension. Results indicate that a microstructure is transformed mainly by the grain boundary sliding process that is responsible for rapid randomization of texture. There is also much evidence for crystallographic slip occurring in conjunction with grain boundary sliding. Accommodation of superplastic flow is linked to increased dislocations density in the lattice. At a threshold level, the dislocation density reaches certain saturation level and the nucleation of voids starts. At this threshold strain, the deformation mechanism is altered and superplastic flow proceeds, however, cavities continue to be produced and coalesce due to the grain boundary sliding process. When the dislocation based accommodation mechanism switches from dislocation based and cavities are formed, the lattice strains begin to recover and no further plastic deformation is introduced into the lattice. The Kernel average misorientation function of OIM was used to indicate the level of strain within the grains to explain the formation of cavities.

Key words: *7475 aluminum alloy, cavitation, residual stress, Kernel average misorientation, GBCD, grain boundary sliding, OIM, superplasticity, texture, X-ray diffraction.*

1. INTRODUCTION

Superplasticity is the ability of certain alloys to undergo high amounts of strain prior to failure. The major deformation mechanism of superplastic deformation (SPD) is the grain boundary sliding (GBS), where grains or packets of grains are observed to change their neighbors and rotate freely. As the grain boundary sliding is widely accepted as the most important mechanism of superplastic deformation the accommodation of flow is still a topic of research that is theorized to be governed by either dislocation motion through glide and climb or diffusion [1-7].

Conventional deformation textures for FCC materials occur because the deformation process takes place on the most favorable slip systems [8]. Hence deformation induces preferential orientation or texture. Typical deformation textures of FCC cold rolled materials are shown in Table 1, which provides the name of the component texture, the {hkl}<uvw> and the corresponding Euler angles in the space of the orientation distribution function (ODF). Deformation textures in FCC materials are also expressed in terms of α and β fibres shown in Figure 1, which strengthen during rolling. The β fibre can be described as a tube which runs from the C component {111}<112> through the S component {123}<634> and finally ends at the B component {110}<112>. The α fibre runs from the B component to the G component {110}<001>. The recrystallization textures of aluminum depend on the alloy composition and the amount of particles present as a second phase [8]. In high purity aluminum, the cube texture is observed as would be expected in high γ_{SFE} materials. But disperzoids or secondary phase particles can pin dislocation motion and deformation textures may remain after recrystallization [8]. In superplastic forming we may observe certain contributions from crystallographic slip deformation and recovery and grain growth during annealing, the mechanisms that were responsible for texture transformation in cold and hot deformation processes. However, because superplastic deformation is governed by grain boundary sliding, texture is expected to be destroyed by superplastic forming. Grain boundary sliding involves the translation and rotation of grains, but this is rather a free rotation that is not controlled by slip and

twinning and not constrained by cold deformation plasticity models and the external boundary conditions [9-10]. Therefore, the GBS process should randomize texture.

Component, Symbol	{hkl}	< uvw >	ϕ_1	Φ	ϕ_2
Copper, C	112	111	90	35	45
S	123	634	59	37	63
Goss, G	011	100	0	45	90
Brass, B	011	211	35	45	90
Dillamore, D	4,4,11	11,11,8	90	27	45
Cube	001	100	0	0	0

Table 1. Major deformation texture components in FCC materials [8]

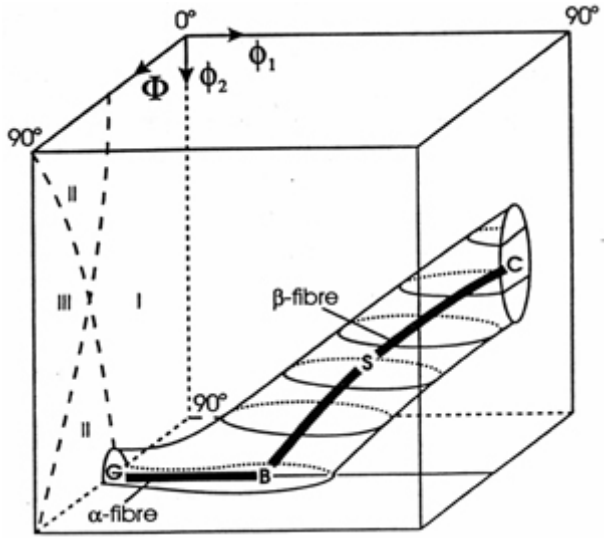


Figure 1. Illustration of the α and β deformation FCC fibres in the ODF space [8].

Certain authors have presented the idea that crystallographic slip may occur at the same time grain boundary sliding [11-13]. It has been suggested that the deformation process is determined by the temperature. At low temperatures crystallographic slip dominates deformation but GBS is also present. At high temperatures, GBS dominates but there is some strengthening of the deformation texture components which are related to contribution from crystallographic slip to deformation. Orientation imaging microscopy (OIM) can contribute to a better understanding of the deformation process of this superplastic alloy, because in addition to changes in texture and grain shape and size and the grain boundaries character distribution, the interaction of grain boundaries with precipitates and residual stress measurements can be performed at different stages of the deformation process. Methods of measuring dislocation activity with OIM are more direct than of other traditional methods, and can provide insight into a more local deformation such as the interior of grains. Recently, techniques have been focused on the image quality (IQ) factor. The image quality factor is directly related to the quality of the EBSP and by consequence to the lattice distortion at a specific point in the scan raster. A reduction in the IQ parameter indicates higher local distortions in the lattice [14]. However, IQ is also dependent on the indexing algorithm and video processing making this parameter less reliable when comparing the internal strains in different samples. To compare the lattice distortion of different samples, the misorientation between points can be used [15,16]. This method compares adjacent EBSPs and provides the angular mismatch between patterns to give the location and the magnitude of distortion in the sample. Since this technique involves the comparison of EBSP's, it is not dependent on the scan conditions effectively enabling the comparison of

multiple samples from different scans. With these new tools, it will be possible to monitor the microstructure, texture and dislocation behavior of the superplastic samples at the microscopic level to gain insight into the accommodation mechanism of grain boundary sliding. Traditional measurements of texture and stress by X-ray diffraction will allow to follow deformation processes at the macroscopic level.

2. EXPERIMENTAL

Strained tensile samples of 7475 aluminum were analyzed. The composition of 7475 is listed in Table 2. R-type [17-19] samples were strained from 0 to 100% in 20% strain intervals at 803K. An additional sample was strained to failure (640%), under the same optimal superplastic conditions set by Takayama et al. [20]. Prior to straining, samples were held at the deformation temperature for 30 minutes. The pulling speed was held constant at 3.3×10^{-6} ms^{-1}. The samples were ground with SiC paper in subsequent step from 240 to 1200 grit and then chemically and mechanically polished in a 0.05 μm colloidal silica bath having a pH of 9 for 6 hours. These steps are essential to remove residual polishing stress.

Element	Zn	Mg	Cu	Cr	Fe	Si	Ti	Al
Wt. %	5.74	2.57	1.50	0.20	0.07	0.04	0.02	Bal.

Table 2. Chemical composition of Al 7475

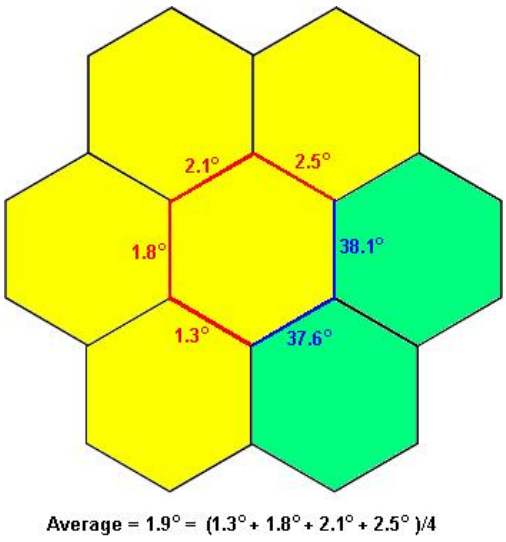


Figure 2. Illustration of the Kernel Average Misorientation function [21]. All of the hexagons represent points in the SEM scan raster. In this case the centre point is under investigation and the Kernel average value for the centre point is found to be 1.9˚

X-ray diffraction experiments were conducted to ascertain global changes in the dislocation density by measuring the peak broadening at each strain interval. The dislocation density was not calculated but trends in peak's broadening behavior were registered. Changes in the peak broadening are due to differences in dislocation activity within the sample. The experiments were performed on a Rigaku Rotaflex D-MAX rotating anode difractometer with Cu Kα radiation (λ = 1.54178 Å). The amperage was set to 130 mA and the voltage maintained at 40 kV. Incomplete (111), (200) and (220) pole figure were measured using a Siemens D-500 texture goniometer with Mo target, operating at 40 kV and 40 mA. These pole figures were used to compute

orientation distribution functions with the use of TexTools v.3.2 software. OIM was used to determine the location and the magnitude of internal lattice distortions as stress accumulated during the deformation process. These experiments were performed on a FEI XL-30 with TSL TexSEM software. The step size was 1 μm and the beam voltage was held constant at 20 keV.

The Kernel average misorientation function was used to determine the lattice distortion. This method involves averaging the misorientation between adjacent EBSPs. In so doing, the average misorientation can be used to map the location and average magnitude of distortion within the grains of the sample. The algorithm rejects misorientations greater than 5° which effectively constrains the calculation to areas within the grains. An example of the technique is shown in Figure 2 [21]. As seen on Figure 2, the centre point is compared to all of its adjacent points. The yellow and green hexagons are the points in the raster corresponding to different grains respectively. As such the Kernel average will compute the misorientation between the centre point and every point surrounding it. If the misorientation angle is greater than 5˚ than the boundary is excluded from the calculation, so as to only consider points belonging to the same grain. Therefore in Figure 2, the Kernel average of the centre point is determined by averaging the misorientation angle of all the red boundaries and associating a value of 1.9˚ to the centre grain. This technique permits to image and locate lattice distortions in the grain interior.

3. RESULTS

3.1. Texture

Figure 3 illustrates the evolution of the intensity of the main texture components with increase of the strain. In the as-received state, the alloy has a strong cube texture, which is a typical texture of recrystallized aluminum [8]. Figure 3 illustrates the rapid randomization of all texture components, which is indicative of grain rotation and translation due to GBS. Randomization is expected because GBS process is dominating in superplastic deformation and this process does not have a crystallographic component which is important in normal cold and hot deformation. Of interest in Figure 2 is the rapidity of randomization of the cube component. Not shown on this figure are the results obtained for the 640% sample, which has a completely random texture. Figure 3 also shows an increasing trend in the intensity of the Brass {110}<112> component. Since this texture component is very weak at the beginning of deformation, the increase illustrates the same randomization trend. The increase of the Brass component illustrates a randomization trend, since in Figure 3, the intensity of all components tends to a similar value. Texture results are presented in Figure 3 using the alpha and beta fibres. It is evident that texture randomization is taking place due to the reduction of the Cube and Goss components. Moreover, the steady brass component increase shown in Figure 3, is well represented in the Beta fibre of Figure 4.

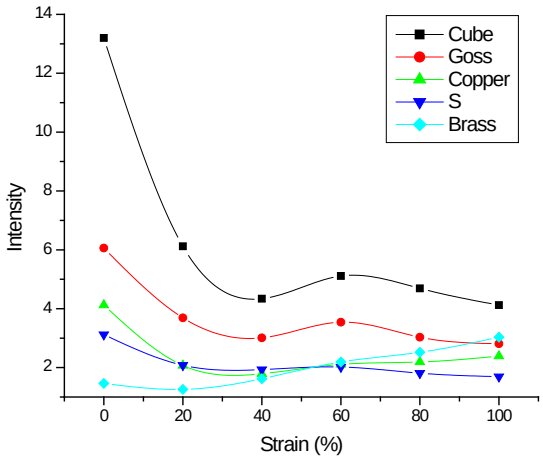


Figure 3. Evolution of texture with respect to strain in superplastic Al 7475

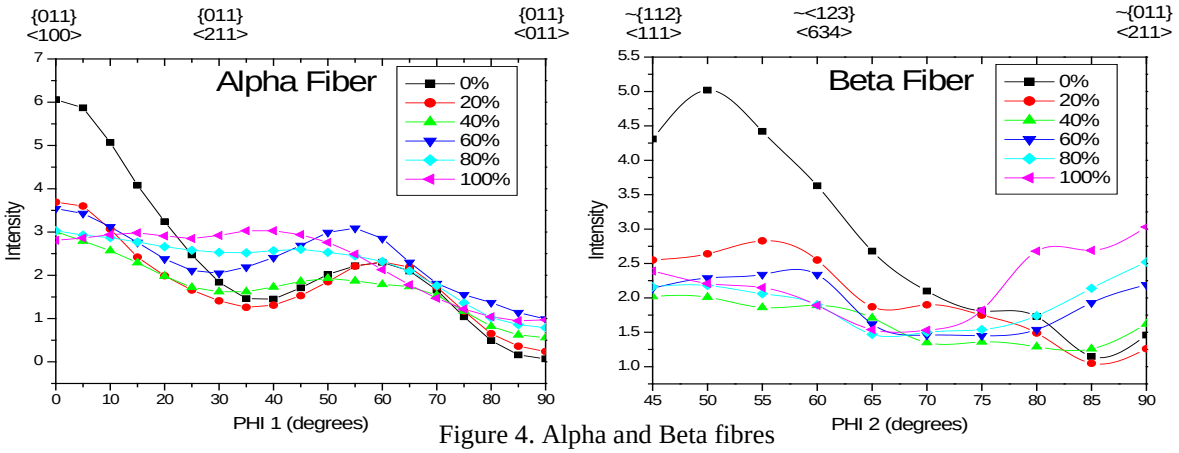


Figure 4. Alpha and Beta fibres

Figure 5, shows the correlated grain boundary character distribution (GBCD) obtained from OIM. As can be seen from this figure the amount of high and low angle grain boundaries remains more or less constant. The GBCD is more or less random and remains as such throughout the deformation process. Variations in the data plotted in Figure 5 are complex to analyze, but could be related to the role of grain boundaries during the grain growth process at the elevated temperature of superplastic forming.

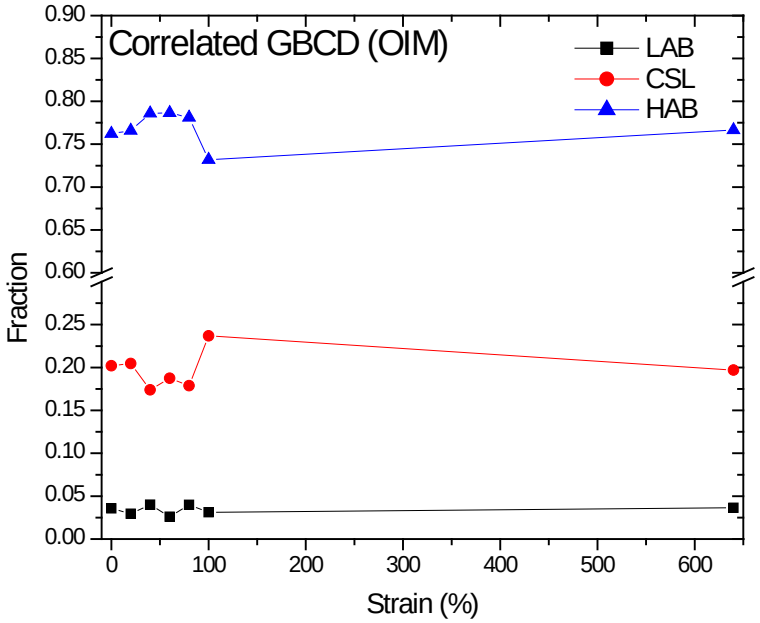


Figure 5. GBCD obtained with OIM. LAB: Low Angle Boundaries 5-15°. HAB: High Angle Boundaries 15-63°. CSL: Coincident Site Lattice boundaries Σ3 to Σ27.

3.2. Microstructure

Figure 6 illustrates the change in the grain size versus strain, which was calculated using OIM to measure the average surface area of the grains and then calculating radius of the circle of the same area. The observed growth follows a parabolic trend with respect to strain. As can be seen from the graph, the growth of the grains occurs throughout the deformation process, which can be expected at elevated temperatures. This increase in the grain size may be associated with plastic deformation of the grains, causing them to elongate, and grain boundary migration which may also increases grain size.

The microstructure of strained superplastic samples is presented in Figure 7. These high contrast back scattered electron micrographs permit to view grain size and morphology. As can be clearly seen from the micrographs in Figure 7, grains become slightly elongated along the tensile axis (marked parallel to the vertical direction of the page) as the level of strain increases. As can be seen from the previous micrographs, there seems to be two fold precipitate behavior within the alloy. Where, coarse precipitates are situated at the grain boundary and finely distributed precipitates are located in the interior of the grains. These precipitates are well document by other authors [9]. The fine precipitates contain chromium and are most likely $Mg_3Cr_2Al_{18}$, while the large precipitates are a combination of phases. It is also clear from the microstructure that the grains tend to elongate towards the tensile direction, which is indicative of grain boundary migration, stress-induced diffusion and some contribution from crystallographic slip. In Figure 7 B-H, a precipitate free zone is formed around growing grains and this zone tends to grow as grain size increases at higher strains. This precipitate free zone is most likely caused diffusion of a solute to the grain boundary where precipitation of that solute at the grain boundary will occur [22]. Moreover, there is strong evidence that plastic deformation and dislocation activity occur in conjunction with GBS, which would enhance the elongation of the grains and the precipitate free zone.

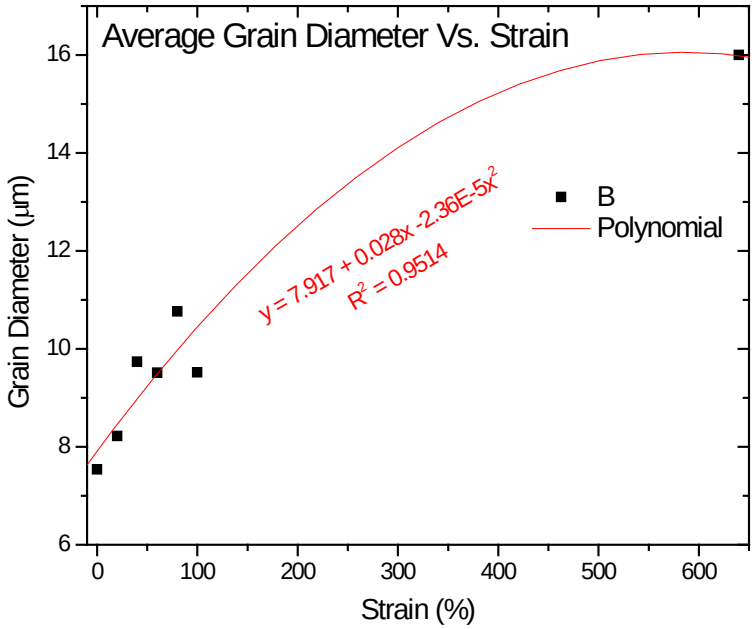


Figure 6. Average spherical grain diameter as measured by OIM with respect to applied superplastic strain

Figure 8 shows the evolution of the aspect ratio of the grains in the microstructure. The aspect ratio is defined as the length of the minor axis of the grain divided by the length of the major axis. Therefore the closer the aspect ratio is to unity the more the grains are equiaxed, the closer the value of the aspect ratio is to zero, the more the grains are elongated. From Figure 8, it is apparent that the grains are being elongated towards the tensile axis as deformation evolves. This may be explained by a combination of grain boundary migration, stress induced mass transport and to some extent may be a consequence of plastic deformation caused by the accommodation process of grain boundary sliding. As can be seen in Figure 7, pores begin to nucleate at triple junctions and grain boundaries when the strain reaches 80%. The amount of porosity in the middle of the gauge length of the samples has been measured by optical microscopy with image analysis software and is presented in Figure 9. As can be seen from this figure there is no porosity before the 80% strain mark. Afterwards, porosity starts to increase in a gradual manner. The large pores observed in the 100% sample in Figure 7G are the result of coalescence during un-accommodated grain boundary sliding. Cavitation results from the inability for matter to remain cohesive, as such, when grain boundary sliding occurs with the absence of the accommodation mechanism, rotation and translation of the grains will produce pores [9]. Because pores start to appear at 80% strain, it can be concluded that the grain boundary sliding accommodation mechanism is ineffective or absent already at this stage of the deformation process.

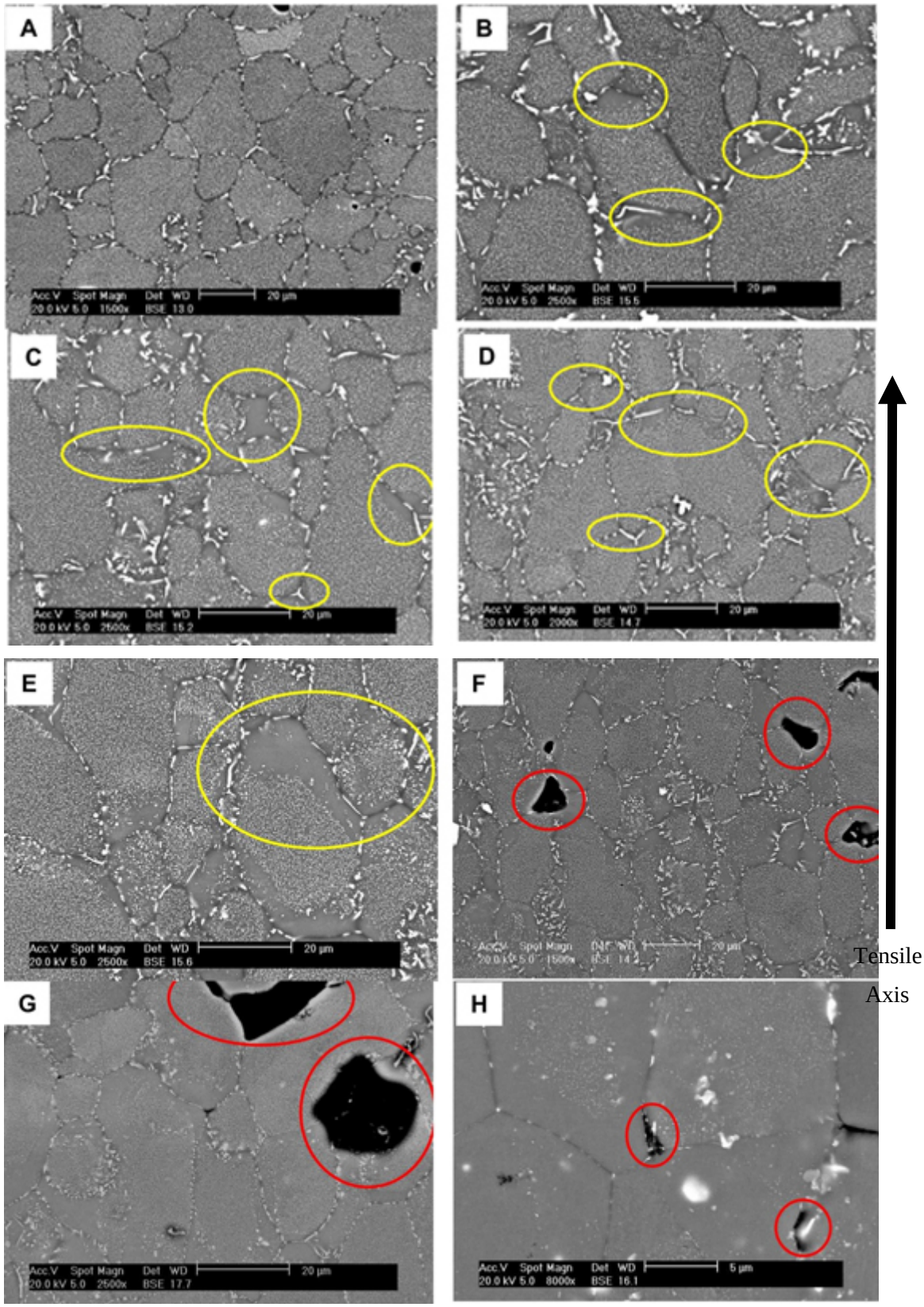


Figure 7. A) Back scattered electron micrograph of the unstrained sample, B) Back scattered electron micrograph of the 20% strain sample, in both cases the tensile axis is parallel to the vertical direction, as marked. Appearance of a precipitate free zone starts at 20% strain, indicated by yellow circles, C) Back scattered electron micrograph of the 40% strain sample, D) back scattered electron micrograph of 60% strain sample, the tensile

direction is parallel to the vertical direction, as marked. Precipitate free zone indicated by yellow circles, E) 80% strain back scattered electron micrograph showing large PFZ's, F) 80% strain micrograph clearly showing the first appearance of porosity, the tensile axis is again parallel to the vertical direction, as marked. Large precipitate free zones marked with yellow circles and appearance of porosity indicated by red circles, G) 100% strain backscattered electron micrograph, H) 640% strain electron micrograph, the tensile direction is parallel to the vertical direction, as marked. Porosity identified by red circles.

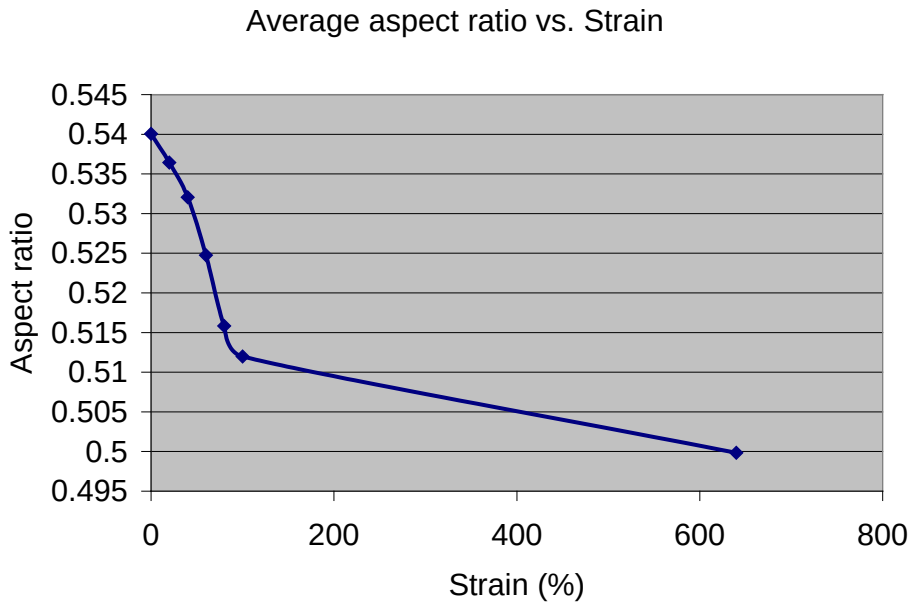


Figure 8. Evolution of the aspect ratio of grains with strain, calculated from OIM micrographs.

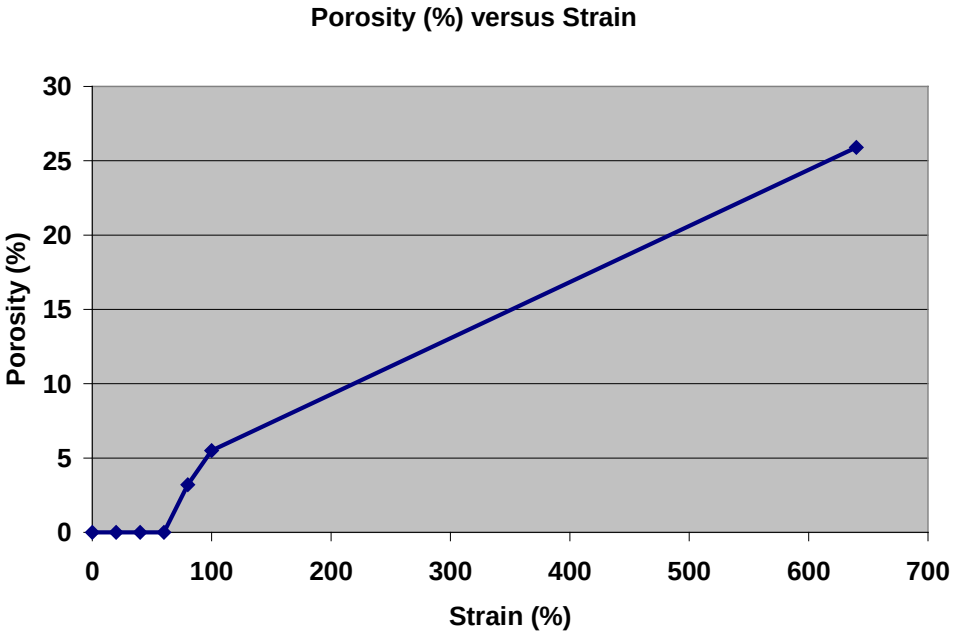


Figure 9. Porosity evolution with strain, ass measured by image analysis with optical microscopy

This results in un-accommodated flow that will generate voids at the grain boundary areas, which can clearly be observed in Figure 7 F and H. Moreover, it is observed in the red circles in Figure 7 F-H that pores are found at interfaces in the microstructure where the precipitate free zone and grain precipitates are located. Since the precipitate free zone is free of precipitates, it is likely that it is easy for it to undergo plastic deformation. If this zone links up with a less plastic area, such as precipitates, it is likely that the local stress concentration would increase. As such, cavitation would occur at these interfaces.

3.3. Residual Stress

Before the voids are formed, considerable stress must be accumulated to nucleate them. This stress, at least partly, should be observed within grains and might be different for grains of different orientation. Figure 10 is a map that illustrates the average misorientation spread for grains in the investigated specimen. These spread values are calculated by averaging the misorientation between all points within the grains, and indicate the extent to which the grains have fragmented and developed substructures. The distributions of this value are also shown for each strain level. From Figure 10, it can be clearly seen that there is a radical transformation in the behavior of internal grain strain from 60 to 80% strain and starting from 80% strain the broadening measured from EBSP patterns increase significantly. This observation is also valid for 640% strain, however at this strain level the internal stresses in several areas are relaxed because the voids are formed and the density of voids increases.

The EBSP observation is also confirmed when investigating the broadening of X-ray diffraction peaks. Figure 11 clearly illustrates the transition from the early stage of deformation (0-60%) to the latter stages (80-640%). It should be remembered that grain boundary sliding takes place at all strains. Therefore the transitional behaviour in internal grain strain may be explained by difference in the accommodation mechanism, which in this case seems to be limited plastic deformation. It would seem that plastic deformation accommodates grain boundary sliding, however at 80% strain some micro voids start to form. At this point the un-accommodated grain boundary sliding occurs and the lattice is free to relax its accumulated stresses at certain locations. Both the X-ray diffraction peaks broadening and the average value of the orientation spread illustrate this trend.

As can be seen from Figure 11, peak broadening follows an increasing trend in the early phase of deformation and then a sudden step change occurs in the broadening behavior followed by a decreasing trend. This trend implies that dislocations are produced during the deformation process and accumulate up to the strain of 80%, which coincides with the strain at which pores start to form. For deformation higher than 80% the internal lattice distortions are observed to relax due to lack of constraints and to the fact that the system is now driven by un-accommodated grain boundary sliding where cavitation more often is “accommodating” the deformation flow. A more localized, approach to the description of transition between low and high strains and stress relief, can be viewed in Figure 12, which shows a Kernel misorientation analysis from 60 to 640% strain. As can be seen, the level of strain in the Kernel misorientation maps echoes that of the broadening behavior in terms of general behavior. Porosity can be clearly seen in Figure 12. Moreover, the initiation of porosity at 80% strain is clearly documented, as well as the coalescence of pores at 100 and 640% strain. In Figure 12, the highest concentrations of lattice distortions are found in the 80% and 100% samples. At 640% the

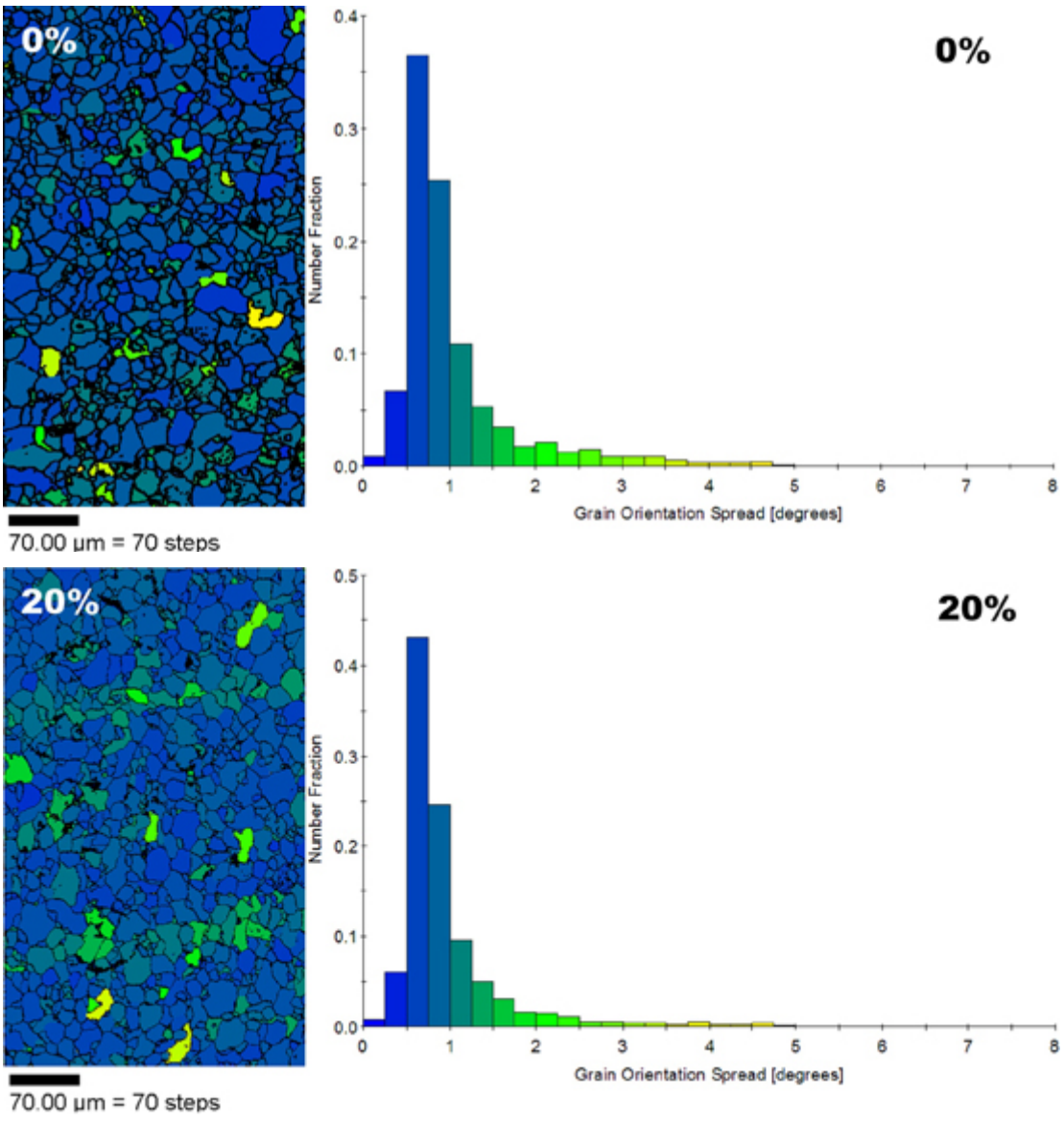
Kernel is more diffuse, again evidence of relaxation of the structure after porosity has appeared. Figure 12 shows a clustering of deformation in which an inhomogeneous distribution of the Kernel misorientation can be observed. It is clear that some clusters of high lattice distortion are concentrated around labeled porosity in 80 and 100% strain samples in Figure 12.

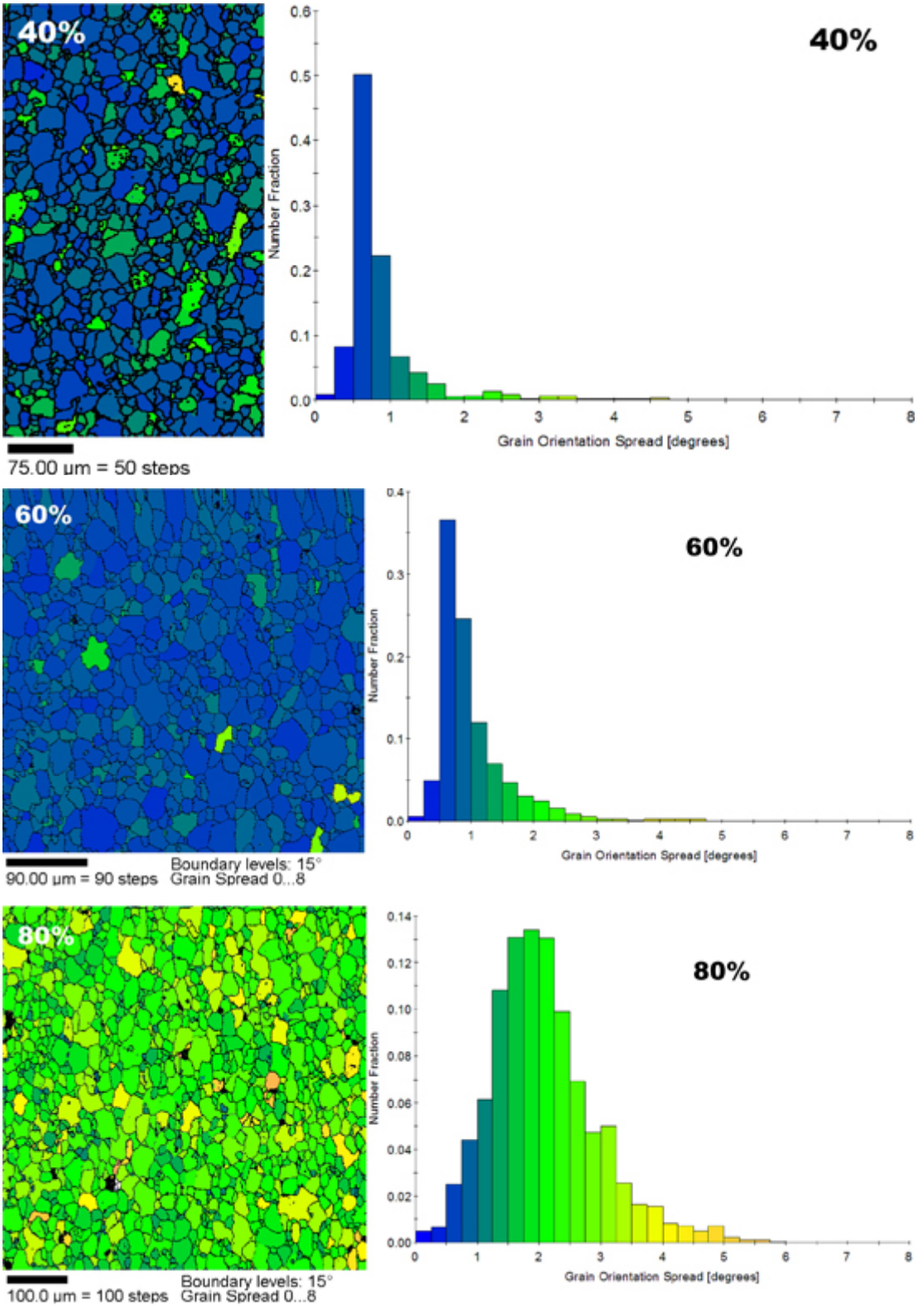
3.4. Precipitation

As mentioned earlier, it has been established that the alloy presents a two fold precipitate distribution. Moreover, a precipitate free zone is formed when GBS evolves. This zone is not present at 0% and appears to grow axis as deformation evolves (Figure 7). Figure 13 presents OIM data and backscatter electron images of the 40 and 80% strain samples. This information is useful to ascertain how precipitates and the precipitate free zone respond to the increased level of lattice distortion caused by deformation. Figure 13 reveals the location of lattice distortion, which can be found either at the interface between the grains (40% b red circle) or in the grain interior around small precipitates (40% b pink circle). This phenomenon is likely due to the presence of crystallographic slip. Dislocations seem to result from the accommodation between two grains during grain boundary sliding. As the lattice becomes more and more strained the dislocations are more prevalent in the grain interior where they are pinned by the small precipitates. In the case of the 40% sample, the effect of the precipitates on the deformation process is that they retard the recovery process by pinning dislocations in the grain interior. This explains why this distortion effect can be observed in the grain interior. It seems that as deformation ensues and the peak amount of lattice strain is reached at 80% strain according to Figure 11, precipitates and the precipitate free zone

Volume 8, ISSN 1314-7269 (Online), Published at: http://www.scientific-publications.net

behave differently. There is definitely more lattice distortion in the grains. This is observed when comparing the 40% b and 80% b kernel maps in Figure 13. There also appears to be large stress concentrations surrounding large precipitates at the grain boundaries, these distortions are seen in the grain, close to the grain boundary, as seen in Figure 13 in the yellow circle. Orientation gradients can be observed between the precipitate free zone and the grain interior as shown by the blue and green circle in Figure 13. The misorientation between the zone and the grain was calculated for certain grains as indicated by the red lines in the 80% sample of Figure 13 (c). The average misorientation between the precipitate free zone and the grain interior has been found to approach ~ 3.5 degrees in these grains. From the orange circles in Figure 13 it can be seen that this particular precipitate free zone has deformed while the grain interior remains unstrained. This is evidence that the precipitate free zone is more plastic than the grain interior, since it has no precipitates, and can easily be deformed to accommodate grain boundary sliding.




40%
40%
Number Fraction
Grain Orientation Spread [degrees]
75.00 µm = 50 steps
60%
60%
Number Fraction
Grain Orientation Spread [degrees]
90.00 µm = 90 steps
Boundary levels: 15°
Grain Spread 0...8
80%
80%
Number Fraction
Grain Orientation Spread [degrees]
100.0 µm = 100 steps
Boundary levels: 15°
Grain Spread 0...8

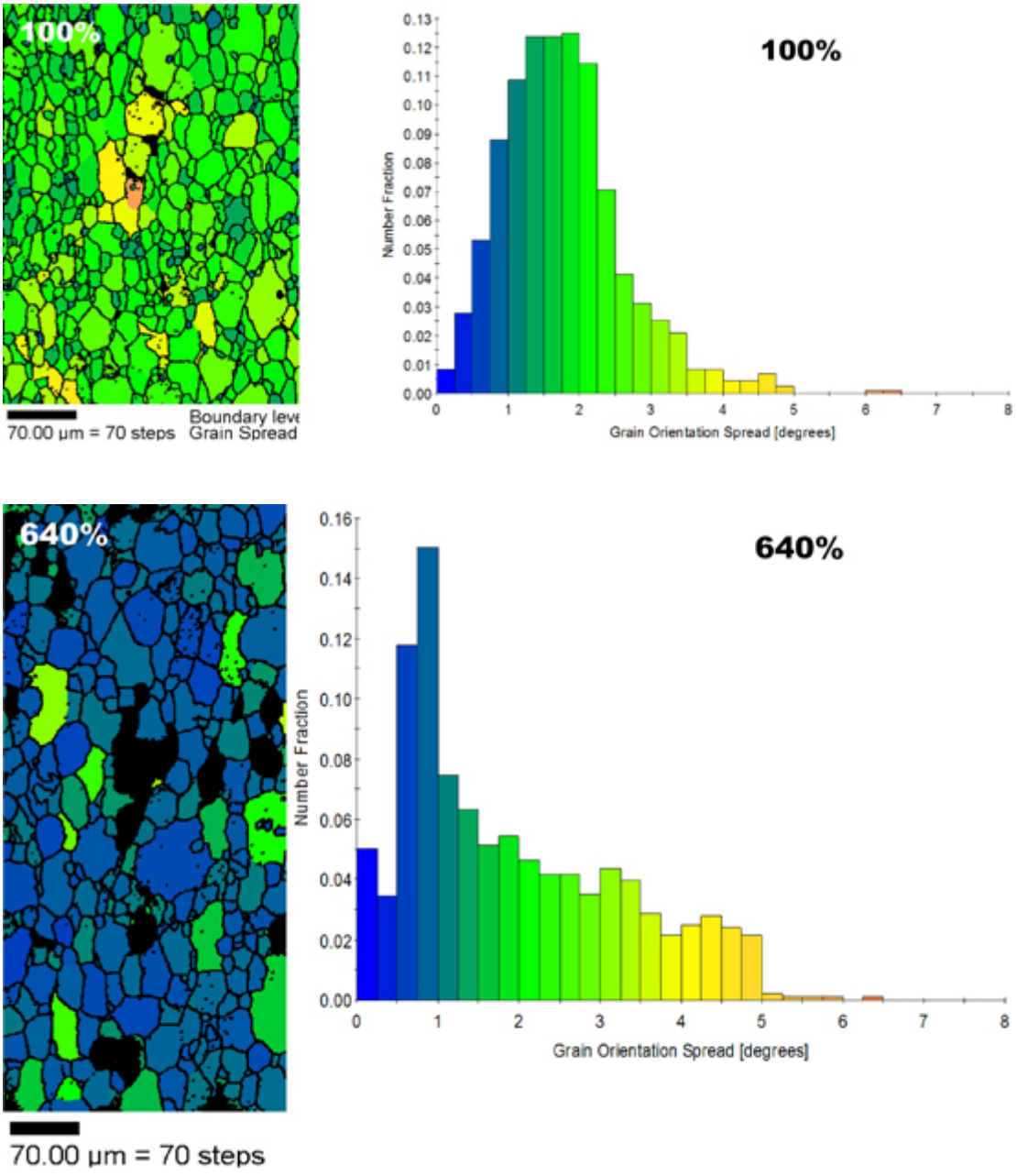


Figure 10: Grain orientation maps and corresponding distributions for 0, 20, 40, 60, 80, 100 and 640% strain.

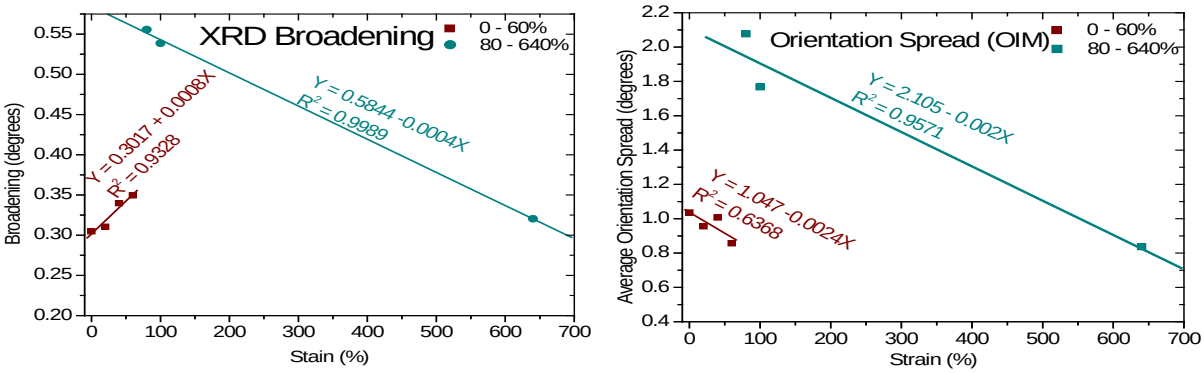


Figure 11. A) X-ray peak broadening as a function of strain, and B) Average value of the average grain orientation spread with respect to strain, both show different behaviors for 0-60% and 80-640% strain.

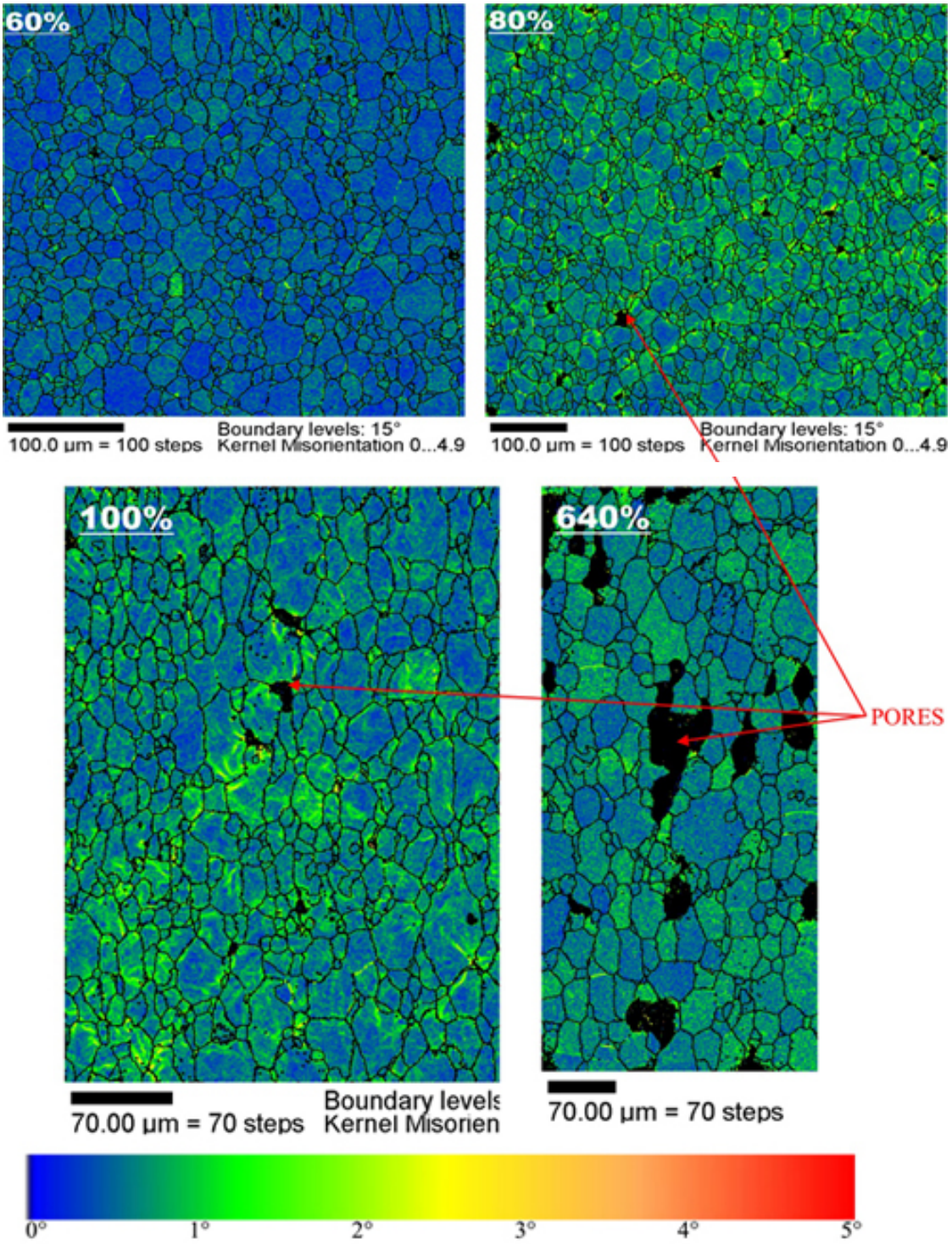


Figure 12. Kernel misorientation maps for the latter strains

4. DISCUSSION

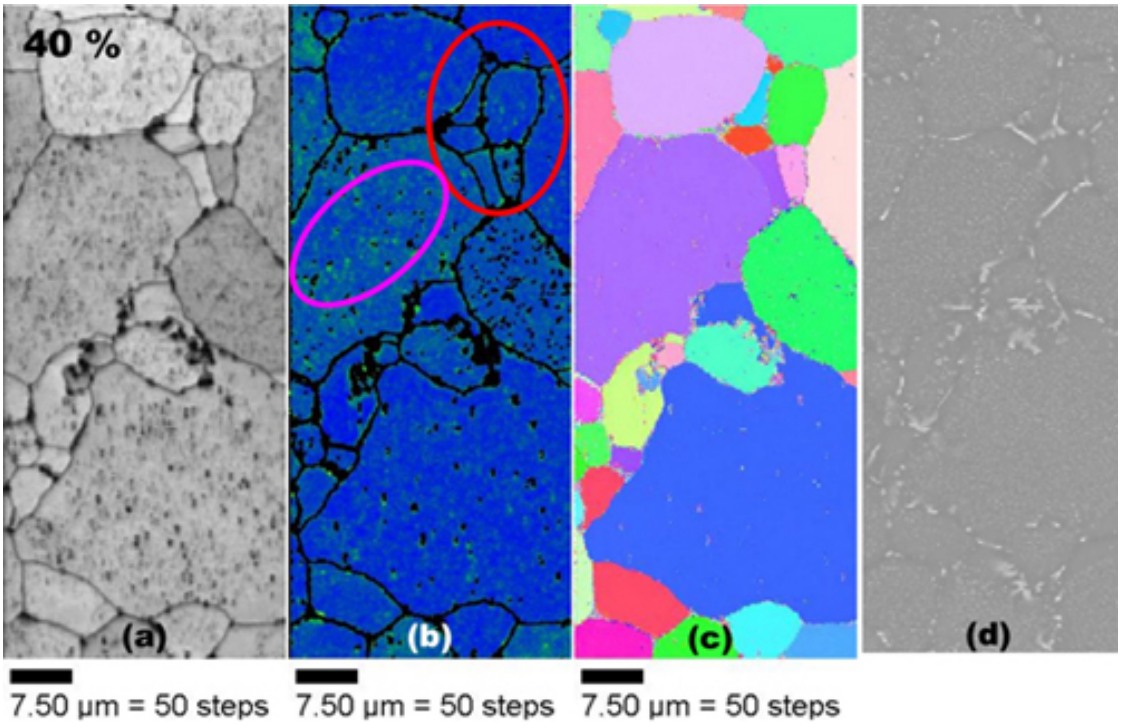
The experiments presented in this article allow us to better understand the processes that contribute to the microstructure transformation during superplastic forming in the investigated 7475 aluminum alloy and comprehend its failure mechanism. The methods used in this investigation can be applied to other materials and in many cases the microstructural changes and interpretation of failure will be similar to described in this article.

Volume 8, ISSN 1314-7269 (Online), Published at: http://www.scientific-publications.net

A rapid randomization of the strong original texture, as observed in Figures 3 and 4 by the lowering the strength of Cube component in particular as soon as deformation begins, is indicative of the occurrence of grain boundary sliding. From the trend illustrated in Figure 3, one may argue that grain boundary sliding is the main deformation mechanism at all strains. The intensities of the major texture components found in the unstrained sample decreases and then reach a lower plateau from the strain of 40% to remain at intensities which are very close to the random state. The initially low intensity components, represented by Brass type texture, increase in strength to the same level of all other components indicating a randomizing of texture. The ODF for the 640% sample is completely randomized, indicating that GBS is occurring throughout the entire deformation process until the specimen fails. It is likely that both crystallographic slip and grain boundary sliding are occurring jointly throughout the early part of the process (0-80% strain), however the crystallographic slip plays mainly a role in accommodation of GBS.

Because pores begin to form in the latter part of the process and the texture of the 640% strain sample in completely random, deformation at this latter stage takes place via un-accommodated GBS. It would seem that when porosity is formed, the mechanism responsible for keeping matter coherent is obviously absent in certain areas of the specimen, which is apparently most often found in the grain boundary area.

The grain boundary character distribution data (Figure 5) presents some variation in the fraction of high angle and low angle boundaries with strain, but overall, there is no evidence of drastic changes in the GBCD's. These results reveal the random state of grain boundaries and cannot offer a statistical argument for preference of sliding of a certain type of the boundaries. Such preference may however exist because the statistical analysis does not include information on the rather complex pattern of concentration of dislocation density around clusters of grains during superplastic forming.



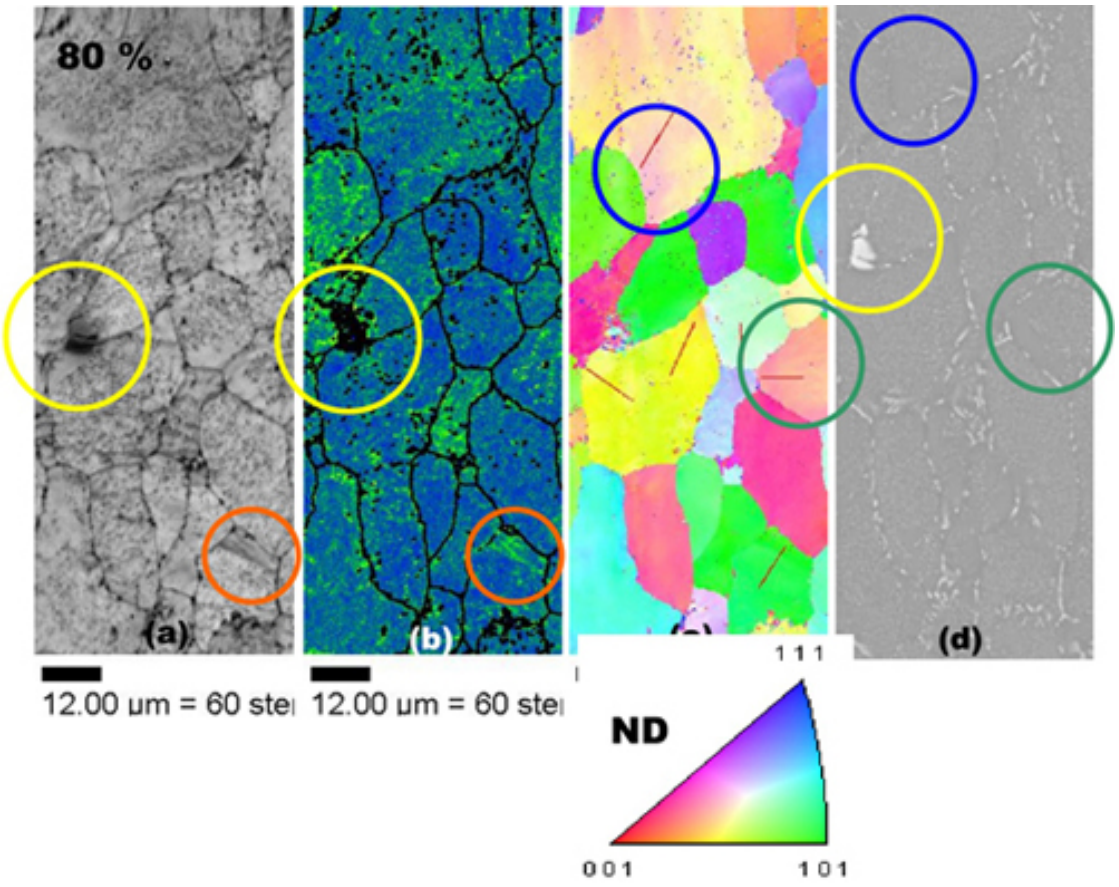


Figure 13. Image quality (a), kernel average misorientation (b), normal direction inverse pole figure (c) corresponding to ND unit triangle, and back scattered electron micrographs (d) of 40% and 80% strain samples, the red lines in 80% (c) represent lines along which misorientation was measured.

Some grain growth during superplastic deformation is expected as a consequence of the high deformation temperatures. It can be clearly seen by Figures 6, 7, and 8 that the grain growth is in effect occurring. Moreover, grain growth seems to follow a parabolic trend illustrated by Figure 6. This implies an inhibition of growth as the samples are being deformed. It is likely that large precipitates that are formed at the grain boundaries contribute to this effect. As grains grow, they also become elongated towards the tensile axis, as illustrated by Figures 7 and 8. The grain elongation is a consequence of plastic strains occurring in the grains and diffusion of atoms from the area under compression to the areas under tension.

Two distinct types of precipitates are readily observed from the high contrast backscattered electron micrographs presented in Figure 7. Large precipitates are found at the grain boundaries while small precipitates are located in the grain interior. The large size class concentrated at the grain boundary is probably responsible for limiting the grain growth and nucleating voids during the grain boundary sliding. It is clear that a precipitate free zone is formed as strain is applied, as seen in Figure 7 within the yellow circles. This zone tends to grow with applied strain and is the result of precipitate coarsening at boundaries of growing grains and highly stressed areas around grain boundaries. At higher strains the precipitate free zone presents an orientation difference with respect to the grain interior, as observed in Figure 13 in the blue and green circles. Since the precipitate free zone's orientation varies with respect to the grain interior by approximately 3.5 degrees, it is likely that it has participated in the accommodation of GBS because it can more easily be deformed to accommodate superplastic flow. The difference between orientations of both zones can be observed in Figure 13 within the blue and green circles. This is also demonstrated by the deformation of the precipitate free zone in the orange circle while the grain interior remains relatively unstrained. The precipitate free zone is observed to grow. The growth of this zone can be explained by a fact that during the grain growth the coarsening of precipitates at the grain boundaries takes place. This coarsening process is facilitated by a high grain boundary diffusion coefficient and accumulation of dislocations around the grain boundaries.

The data from Figures 10-13 suggest that lattice distortions are accumulating as strain is increased, in conjunction with the grain boundary sliding process. Grain boundary sliding is the major deformation mode, and strain is accumulated as a result of the sliding and rotation of grains. To accommodate the applied strain, significant local differences in lattice distortion and dislocation densities are generated and such differences are responsible for the nucleation of pores. These are well illustrated in Figures 7, 9, 10 and 12. In Figure 13 one can see that the lattice distortions are concentrated in the precipitate free zone as well as in the grain interior. Moreover, distortion clustering is observed around pores in Figure 12, implying that this concentration of dislocations lead to the formation of cavities. Once cavitation occurs it relaxes the internal strain as it can be seen in Figures 10-12. The appearance of cavitation on OIM images coincides with changes in the broadening of the X-ray diffraction peaks, the X-ray peak broadening is decreased and the kernel average misorientation is more diffuse in the 640% sample. All of these facts point to the relaxation of the lattice distortion and are linked to the appearance and growth of pores. Moreover, from the tail end of the 640% Kernel spread misorientation distribution shown in Figure 10, we see that the broadening may have decreased, but the number fraction of grains accumulating high misorientation of above 3.5 degrees has increased comparing to the 100% distribution. This implies that plastic deformation still occur and is significant in certain areas where the flow is un-accommodated.

As soon as cavitation starts the average lattice stress begin to recover. The phenomenon is illustrated in Figure 11 where in the 80-640% strain range the magnitude of the misorientation spread distribution decreases and the broadening at half maximum deceases. This effect is well illustrated by significant dithering of the kernel average misorientation in the 640% sample, which is evidence of recovery of the lattice distortions. This implies that the bulk of the structure is relaxed by the formation of pores. Preferential relaxation is adjacent to formed pores, where the grains are unconstrained. The lattice distortion in some grains actually increases in particular for the highest strain of 640%.

The precipitate free zone can be more easily deformed than the bulk of the grains. Moreover recovery and softening of the zone would be easier than of the area with precipitates. This situation would lead to incremental slip and recovery, which would accommodate GBS. Once porosity appears GBS is not well accommodated. The structure is strained further and more pores will be generated. This is well illustrated in Figure 9. Comparing Figures 9 and 11, it is evident that the pores are formed at the area where the lattice distortion is concentrated. As deformation evolves the level of porosity increases while the level of residual strain decreases. Porosity is nucleated at the interface between precipitates and the precipitate free zone. It is well known that porosity will first be formed in the area with the highest stress concentration. This would be often at the triple junctions [23], as seen in Figure 7 H. As can be seen in Figure 13, the inverse pole figure maps illustrate difference in deformation behaviour between the PFZ and the grain interior. If this relatively plastic zone encounters precipitates, the stress concentration at this interface would increase and lead to voiding. This may be one of the factors that lead to formation of pores at the interface of the PFZ and harder area with precipitates. Ultimately, the coalescence of cavitation, as observed in Figure 12 at 640% will result in failure. Coalescence of pores is expected once the GBS accommodation fails.

5. CONCLUSIONS

1) Randomization of texture indicates that grain boundary sliding is the most important deformation process. However, increase in the X-ray peak breadth, grain elongation and Kernel misorientation indicate that crystallographic slip occurs in conjunction with grain boundary sliding. This strongly implies that accommodation of grain boundary sliding favours increases in the dislocation density in the microstructure. Therefore, the accommodation mechanism may be governed by local deformation and diffusion process.

2) Difference in the deformation behaviour at the interface of the PFZ and the zone with precipitates lead to increased stress concentrations in these interface areas and the formation of pores. Once pores appear, residual strain in the lattice is relieved. Grains adjacent to a pore can freely relax reliving distortion incurred during the deformation process. Although the lattice stress is largely relieved, some grains are still heavily distorted, implying that dislocations are still introduced into the lattice. Ultimately, as deformation ensued in the un-accommodated GBS mode, pores will coalesce and the alloy will fail.

3) Due to orientation differences between the grain interior and the precipitate free zone, the zone can be linked to the accommodation mechanism. This zone is easier to deform than the grain interior and can accommodating GBS by dislocation motion.

4) The formation of precipitate free zone is mainly governed by high diffusivity of grain boundaries that facilitate the precipitation coarsening at the grain boundary. The stress accumulated at the grain boundary region contributes to higher diffusivity of this region and facilitates the precipitate coarsening. Large precipitates are concentrated at the grain boundaries and small precipitates in the grain interior. The precipitates inhibit grain growth and may pin dislocation movement in the grain interior.

5) Evidence of dislocation activity was obtained using the Kernel average misorientation function on OIM and X-ray diffraction peak broadening. Based on these, the magnitude and location of dislocation activity within the grains can be determined.

REFERENCES

Ashby, MF & Verrall, RA 1973, 'Diffusion-accommodated flow and Superplasticity', *Acta Metallurgica*, vol. 21, pp.149-159.

Spingarn, JR & Nix, WD 1978, 'Diffusional creep and diffusionally accommodated grain rearrangement', *Acta Metallurgica*, Vol. 26, pp.1389-1398.

Ball, A & Hutchison, MM 1969, 'Superplasticity in the Aluminum - Zinc Eutectoid', *Metal Science Journal*, vol. 3, pp. 1-6.

Langdon, TG 1971, 'Grain boundary sliding as a deformation mechanism during creep', *Philosophical Magazine A*, vol. 22, pp. 689-700.

Mukherjee, AK 1971, 'The rate controlling mechanism in superplasticity', *Materials Science and Engineering*, vol. 8, pp.83-89.

Gifkins, RC 1976, 'Grain boundary sliding and its accommodation during creep and superplasticity', *Metallurgical transactions A*, vol. 7, pp.1225-1232.

Fukuyo, H, Tsai, HC, Oyama, T, & Sherby, OD 1991, 'Superplasticity and Newtonian-viscous flow in fine-grained class 1 solid solution alloys', *ISIJ International*, Vol. 31, pp. 76-85.

Humphreys, FJ, & Hatherly, M 1995, *Recrystallisation and related annealing phenomenon*, Pergamon Press.

Pilling, J, & Ridley, N 1989, *Superplasticity in Crystalline Solids, The Institute of Metals*, London.

Edington, JW, Melton, KN, & Cutler, CP 1976, 'Suerplasticity', *Progress in Materials Science*, Vol. 21, pp. 63-170.

Perez-Prado, MT, Cristina, MC, Ruano, OA & Ganzalez-Doncel, G 2000, 'Study of the deformation mechanisms of the superplastic alloy Al-Li 2090 by texture analysis', *Textures and Microstructures*. Vol. 34, pp. 205-216.

Perez-Prado, MT & Gonzalez-Doncel, G 2000, 'Texture changes during deformation of 7475 superplastic aluminum sheet alloy', *Textures and Microstructures*, Vol. 34, pp.33-42.

Perez-Prado, MT, Cristina, MC, Ruano, OA, & Gonzalez-Doncel, G 1998, 'Grain boundary sliding and crystallographic slip during superplasticity of Al-5%Ca-5%Zn as studied by texture analysis', *Materials Science Engineering A*, Vol. 224, pp. 216-223.

Randle, V, & Engler, O 2000, *Introduction to Texture Analysis Macrotexture, Microtexture & Orientation Mapping*, Overseas Publishers Association.

Wilkinson, AJ 2000, 'Measuring Strains using Electron Backscatter Diffraction', in *Electron backscattered diffraction in material science*, Kluwer academic, Chapter 20, pp.231-246.

Lehockey, EM, Lin, Y, & Lepik, OE 2000, 'Mapping residual plastic strain in materials using electron backscattered diffraction', in *Electron backscattered diffraction in material science*, Kluwer academic, Chapter 20, pp.247-264.

Takayama, Y, Fushiro, N, Tozawa, T, & Kato, H 1994, 'New Method for Evaluation of Superplastic Characteristics Using the R-Type Specimen', *Materials Science Forum*, Vol. 170-172, pp. 561-570.

Takayama, Y, Tozawa, T, Kato, H, & Fushiro, N 1997, 'Usefulness of the R-type specimen method for evaluation of superplastic characteristics in a 7475 aluminum alloy', *Materials Science Forum*, Vol. 233-234, pp.117-122.

Mizunuma, S, Takahashi, H, Tkayama, Y, Fushiro, N, & Mimaki, T 1999, 'Advanced Technology of Plasticity', *Proceedings of the 6th ICTP*, 19-24 September.

Takayama, Y, Tozawa, T & Kato, H 1999, 'Superplasticity and the thickness of liquid phase in the vicinity of the solidus temperature in a 7475 aluminum alloy', *Acta Materialia*, Vol. 47, pp. 1263-1270.

TexSEM Laboratories 1998, *OIM™ Analysis For Windows User Manual*, Draper, Utah, USA.

Shin, DH, Joo, YJ, Kim WJ, & Lee, CS 1998, 'Microstructural evolution during superplastic deformation of a 7475 Alloy', *Journal of Materials Science*, Vol. 33, pp. 3073-3078.

Chen, CL, & Tan, MJ 2002, 'Effect of grain boundary character distribution (GBCD) on the cavitation behaviour during superplastic deformation of Al 7475', *Materials Science Materials A*, Vol. 338, pp. 243-252, 2002.